Modelling photosystem I as a complex interacting network: Modelling the photosynthetic system i as complex interacting network

INTERFACE

royalsocietypublishing.org/journal/rsif

Research

Cite this article: Montepietra D, Bellingeri M, Ross AM, Scotognella F, Cassi D. 2020 Modelling photosystem I as a complex interacting network. *J. R. Soc. Interface* **17**: 20200813.
http://dx.doi.org/10.1098/rsif.2020.0813

Received: 9 October 2020
Accepted: 20 October 2020

Subject Category:
Life Sciences–Physics interface

Subject Areas:
bioinformatics, biophysics

Keywords:
complex network, photosystem I, photosynthetic network, biological network, network robustness, network attack

Author for correspondence:
M. Bellingeri
e-mail: michele.bellingeri@polimi.it

Electronic supplementary material is available online at https://doi.org/10.6084/m9.figshare.c.5194156.

THE ROYAL SOCIETY PUBLISHING

Modelling photosystem I as a complex interacting network

D. Montepietra[1,2], M. Bellingeri[3,4], A. M. Ross[4], F. Scotognella[4,5] and D. Cassi[3]

[1]Dipartimento di Fisica, Università di Modena e Reggio Emilia, via Campi, 213/a, 41125 Modena, Italy
[2]CNR NANO S3, Via Campi 213/A, 41125 Modena, Italy
[3]Dipartimento di Scienze Matematiche, Fisiche e Informatiche, Università di Parma, via G.P. Usberti, 7/a, 43124 Parma, Italy
[4]Dipartimento di Fisica, Politecnico di Milano, Piazza Leonardo da Vinci 32, 20133 Milano, Italy
[5]Center for Nano Science and Technology@PoliMi, Istituto Italiano di Tecnologia, Via Giovanni Pascoli, 70/3, 20133 Milan, Italy

MB, 0000-0002-5729-1123

In this paper, we model the excitation energy transfer (EET) of photosystem I (PSI) of the common pea plant *Pisum sativum* as a complex interacting network. The magnitude of the link energy transfer between nodes/chromophores is computed by Forster resonant energy transfer (FRET) using the pairwise physical distances between chromophores from the PDB 5L8R (Protein Data Bank). We measure the global PSI network EET efficiency adopting well-known network theory indicators: the network efficiency (Eff) and the largest connected component (LCC). We also account the number of connected nodes/chromophores to P700 (CN), a new ad hoc measure we introduce here to indicate how many nodes in the network can actually transfer energy to the P700 reaction centre. We find that when progressively removing the weak links of lower EET, the Eff decreases, while the EET paths integrity (LCC and CN) is still preserved. This finding would show that the PSI is a resilient system owning a large window of functioning feasibility and it is completely impaired only when removing most of the network links. From the study of different types of chromophore, we propose different primary functions within the PSI system: chlorophyll *a* (CLA) molecules are the central nodes in the EET process, while other chromophore types have different primary functions. Furthermore, we perform nodes removal simulations to understand how the nodes/chromophores malfunctioning may affect PSI functioning. We discover that the removal of the CLA triggers the fastest decrease in the Eff, confirming that CAL is the main contributors to the high EET efficiency. Our outcomes open new perspectives of research, such comparing the PSI energy transfer efficiency of different natural and agricultural plant species and investigating the light-harvesting mechanisms of artificial photosynthesis both in plant agriculture and in the field of solar energy applications.

1. Introduction

The ability of photosynthetic oxygenic organisms to convert light energy into chemical energy depends on a group of large membrane-bound complexes whose coordinated activity allows the capture of photons and their conversion into highly energetic molecules as NADPH and ATP through an electron transport chain [1]. The whole photosynthetic process is driven by the biological complexes possessing the light-capturing function: photosystem I (PSI) and photosystem II (PSII) [2,3]. It starts with the absorption of photons by PSII that uses them to oxidize water. The oxidation of water produces oxygen and reduces membrane-embedded quinones that are then used by the cytochrome b_6f complex to create a proton gradient across the membrane and to reduce the small copper protein plastocyanin (PC), that is the electron donor of PSI. After absorption of additional photons by PSI, oxidation takes place and the removed electron migrates to reduce ferredoxin (Fd). Eventually, reduced Fd

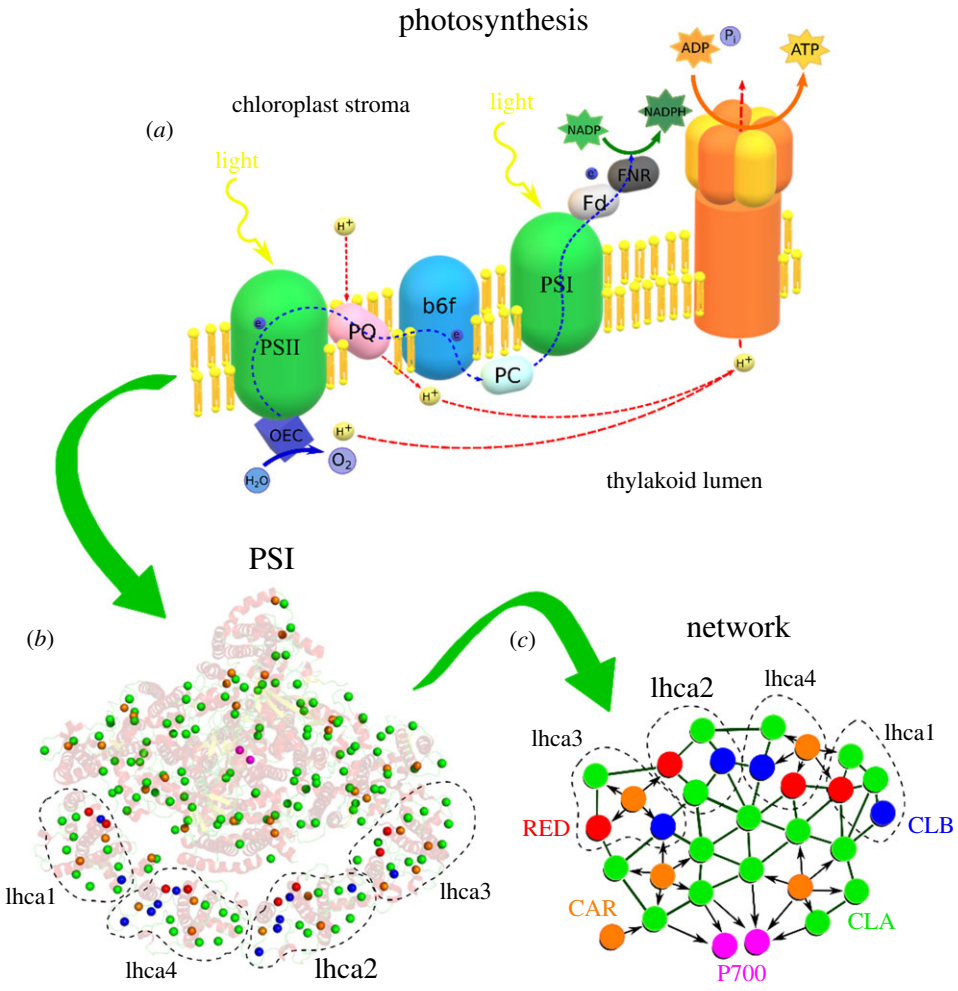

Figure 1. (*a*) Schematic representation of the different protein complexes and the mechanisms involved in the photosynthetic process. In order, from left to right, we find: OEC, oxygen evolving complex; PSII, photosystem II; PQ, plastoquinone pool; b6f, b6f cytochrome; PC, plastocyanin; PSI, photosystem I; Fd, ferrodoxin; FNR, ferrodoxin NADP (+) reductase; ATP-synthase. (*b*) Representation of the PSI network nodes embedded in the 3D protein structure. Node colour indicates the different PSI network chromophores as in the right figure scheme (*c*). The four lhcas are surrounded with dashed lines. (*c*) Schematic of the different nodes of the PSI network and their connectivity. CAR (orange) can only be starting nodes, thus they have only outgoing links. We underline that every node can be the starting point of EET, but CAR can only have outgoing links because of their higher site energy. Chlorophyll *a* molecules (CLA, green) can have both outgoing and ingoing links, as chlorophyll *b* (CLB, blue) and red-shifted chlorophyll forms RED (red). Finally, P700 (magenta) is the point of arrival of the EET process and only possesses ingoing links. The two P700 chlorophylls are not directly connected.

will reduce $NADP^+$ to NADPH that will power the Calvin cycle to produce carbohydrates [4]. The photosynthetic process is schematically depicted in figure 1*a*.

Within the light-harvesting biological complexes PSII and PSI, light is absorbed and transferred to a reaction centre (RC) through a highly efficient excitation energy transfer (EET) [5]. The two photosystems display a common structural organization and two main functional moieties: a core complex, containing the RC where the photochemical reactions occur (called P700 for the PSI), and a peripheral antenna system devoted to the increase in the light-harvesting capability and to the regulation of the photosynthetic process [4,6,7].

The core complexes have been well conserved during evolution, as most of the subunits are similar in prokaryotic and eukaryotic photosystems and only a few are specific to each group [8]. On the contrary, the peripheral antenna system displays great variability, being composed of peripheral-associated membrane proteins in cyanobacteria, called phycobilisomes, and integral light-harvesting complex (LHC) membrane proteins in eukaryotic cells [9].

The light-harvesting process and the EET from the antenna complexes to the RC are facilitated by pigment–protein complexes (PPCs). In green plants (Viridiplantae), most of the light is absorbed by the photosynthetic pigments chlorophyll *a* and *b*, allowing efficient light harvesting and ultrafast EET among antenna chlorophylls, leading to the quantum and thermodynamic efficiencies that are the highest known [9,10].

Also, chlorophylls (Chls) absorbing at energy lower than the P700 are present. Although these spectral forms (called red form Chls) account only for a small percentage of the total absorption, their effect in the energy transfer and trapping of PSI is very prominent [11], with at least 80% of excitation in the PSI transiting through them on their way to the RC [12]. As red form Chls cause most of the energy to be stored at energies lower than that of the RC, this means that energy must travel up-hill prior to charge separation, slowing down the EET process [12]. Despite the potentially slowing down role of the red form Chls, PSI is known to be the most efficient light converter in nature, with a quantum efficiency close to 1 [13,14].

Other cofactors present in PSI are also involved in the processes of light capturing, charge separation and prevention of photodamage, as carotenes. This network of pigments, whose absorption spectra spans a broad spectral range, is embedded in a protein scaffold which enforces chromophores spatial organization by holding them in a relatively rigid position and orientation [3].

Most of the research conducted on the PSI has focused on understanding the chemistry underlying the electron transfer in the RC [15–21]. Nonetheless, reduced efforts have been directed to investigate how the whole chromophores topological structure may affect the high EET efficiency of the PSI system [2,3].

The purpose of this research is to fill the gap, by focusing on the global topological structure of the PSI chromophores system. To address this point, we analysed the structural organization of a plant PSI as a complex networked system for EET adopting the network science viewpoint. Network science has proven to be a powerful tool for the study of complex systems from many different realms [22–30]. Basically, a network is a model composed by nodes (or vertices) and links (edges), where nodes indicate the components of the system and the links define the interactions among them [31,32]. Here, we model the PSI light-harvesting system of the plant *Pisum sativum* as a complex network of nodes/chromophores describing the energy transfer links among them.

First, we find that the PSI is a highly connected network with very short EET pathways from the nodes harvesting the light to the RC. Second, we discover that the capacity to perform EET in the whole network is severely impaired only by removing the majority of EET links. This unveils the high resilience of the PSI system, which holds the capacity to perform energy transfer in the whole network even reaching severe conditions for its feasibility. Last, we simulate different scenarios of chromophores malfunctioning by removing nodes from the network using node attacks strategies framework [22,33]. We find that the removal of chlorophyll *a* is clearly more harmful in decreasing PSI functioning, suggesting these chromophores as the key structural component of the high efficiency EET in the PSI of the *P. sativum*.

2. Methods

2.1. Network theory

A generic network (or graph) $G(N, L)$ is composed by a set of N nodes and L links connecting them. The network G can be abstracted in $N \times N$ square adjacency matrix A, where the element $a_{ij} = 1$ indicates the presence of a link between node i and node j and 0 otherwise [31]. In the case G is undirected, e.g. the links have no directionality, the adjacency matrix is symmetrical with $a_{ij} = a_{ji}$. In a directed network, the adjacency matrix is not symmetrical, the links own proper direction and $a_{ij} = 1$ stands for a link from i to j, and $a_{ji} = 1$ indicates that the link goes from j to i. In the case, the links among nodes are only present–absent, as in G above described, the network is called binary or topological or unweighted. Nevertheless, many real networks are naturally weighted displaying a large heterogeneity in the capacity of the links/connections. In fact, in weighted networks, links are associated with weight values that differentiate them in terms of their strength, intensity or capacity [23,26,34–37]. Thus, a weighted network can be abstracted by a $N \times N$ weighted adjacency matrix W, where the element $w_{ij} > 0$ in the case, there is a link of weight w_{ij} between node i and node j and $w_{ij} = 0$ otherwise. Many empirical studies have demonstrated that purely binary-topological models are inadequate to explain the complex structure of real systems, and that there is a need for weighted network models to overcome the simple topological description [31,32,38].

2.2. Building the photosystem I network

We built the PSI network of the common pea plant (*P. sativum*) starting from the PDB (Protein Data Bank) entry 5L8R [4]. We modelled PSI as a weighted directed network of N nodes/chromophores and L links/FRET efficiencies. The nodes represent chromophores with different identities, i.e. chlorophyll *a*, chlorophyll *b*, β-carotene and derivates, lutein, violaxanthin (figure 1*b*).

We distinguished the different chromophores under five node categories, each one with a specific role in the EET mechanism:

1. P700: RC special chlorophyll pair associated with the PSI.
2. RED: red-shifted form of chlorophyll *a*, concentrated in the LHCI complex.
3. CLA: chlorophyll *a* molecules that do not belong to P700 or RED (PDB Ligand ID: CLA).
4. CLB: chlorophyll *b* molecules (PDB Ligand ID: CHL).
5. CAR: the different carotenoids are β-carotene and derivated molecules, lutein, violaxanthin (PDB Ligand IDs: BCR, ZEX, LUT, XAT, respectively).

To model the PSI network, we assumed that all chromophore molecules can be summarized by one of their atoms. The different types of chlorophyll molecules (PDB categories P700, RED, CLA, CLB, altogether called Chls) are represented using their Mg atom, a common practice in the literature [5,39]. In this way, we found 156 Chls molecules in the PSI complex (12 CLA, 134 CLA, two P700 and eight red forms). Molecules belonging to the CAR category are long conjugated molecules with electrons delocalized in the entirety of the molecule, thus the internal processes are much faster than the external ones (i.e. energy transfer) [40]; for this reason, we consider each CAR as a point/node object delivering energy in the system. We chose the C_{15} carbon, located in the middle of the molecule, to represent the CAR chromophores. Thirty-six nodes belong to the CAR category. Altogether, we obtain a PSI network with a total number of nodes $N = 192$ (table 1).

The feasibility of the energy transfer among a nodes/chromophores in the PSI depends on their nature [41,42]. For this reason, the link directionality connecting nodes in the PSI network also depends on the different nature of the connected chromophores. To assign link directions among chromophores, we followed the energy scheme reported by Croce and Van Amerongen [41] (figure 2). Based on the directionality of the links, we have nodes with outgoing link only (CAR), nodes with incoming links only (P700) or nodes with both directionalities of the links (CLB, CLA, RED). Consequently, some types of links among nodes/chromophores types are forbidden: CLA → CAR, CLB → CAR, RED → CLB, RED → CAR, CAR → CAR.

To assign link weights, we assumed that the underlying mechanism of energy transfer (EET) between all the nodes/chromophores is represented by Forster resonant energy transfer (FRET) [43]. FRET contributes to most of the EET acting as a good approximation to investigate energetic coupling of the underlying spatial organization of the chromophores [44,45]. For the sake of simplicity, we, therefore, assumed that the distance between chromophores is the only parameter affecting the transfer efficiency between them. This approximation is motivated by the fact that the distance between chromophores affects the efficiency of energy transfer in inverse proportion to its sixth power, while the orientation affects only about three times. Future

Table 1. Summary of the different nodes/chromophores of *P. sativum* PSI network.

molecule identity (PDB ligand ID)	node category	number	biological function	link direction
–β-carotene (BCR) –β-carotene and β-carotene derivates (ZEX) –lutein (LUT) –violaxanthin (XAT)	CAR	36	photodamage protection; lower wavelength absorption; energy transfer	outgoing
chlorophyll *a* (CLA)	CLA	134	energy transfer	outgoing + ingoing
chlorophyll *b* (CHL)	CLB	12	light harvesting; wider harvested light spectrum; energy transfer	outgoing + ingoing
red form chlorophylls	RED	8	long wavelength absorbing spectral form of chlorophylls; wider harvested light spectrum; energy transfer	outgoing + ingoing
P700	P700	2	reaction centre of PSI, special pair of chlorophylls	ingoing

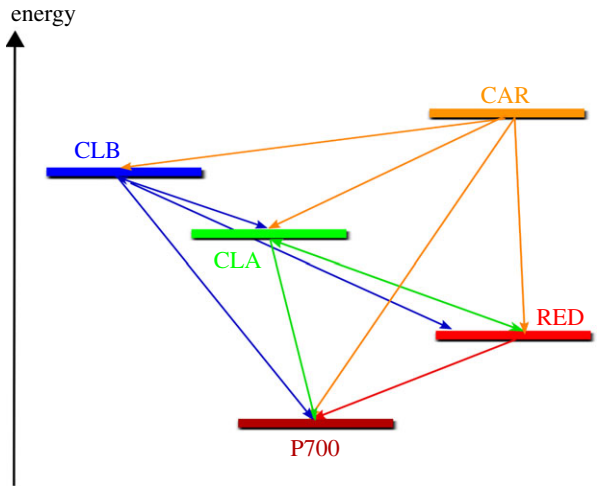

Figure 2. Energy scheme and possible connections between nodes used for the construction of the PSI network, figure adapted from Croce and van Amerongen [41].

investigations may expand the model presented here by including the quantum mechanical dynamics to model the EET of the PSI.

Link weights are assigned using the FRET efficiency:

$$E_{ij} = \frac{1}{1 + (r_{ij}/R_0)^6}, \tag{2.1}$$

where E_{ij} is the FRET efficiency of the link connecting nodes i and j, R_0 is the Forster distance between i and j and $r_{i,j}$ is the physical distance between the nodes. All pairwise physical distances between nodes can be calculated directly from their PDB spatial coordinates. The value of R_0 changes according to the nature of the connected nodes i and j. The values of R_0 between CLA → CLA, CLA → P700, CLB → CLA, CLB → P700, CAR → CLA and CAR → P700 have been obtained directly from the literature [45–48]. The R_0 of all CAR molecules towards other types of chromophores is approximated by the R_0 of BCR [48]. R_0 for CLA → CLB is calculated considering that the Forster rate of CLA → CLB is approximately 1/16 of CLB → CLA [41]. R_0 for RED → CLA and RED → P700 was derived from Cinque *et al.* [49]. For other R_0 without an experimental value from the literature, we made the following assumptions, based on the similarities between the chromophores involved in the links:

— CLA → RED, RED → RED are the same as CLA → CLA and CLA → P700.
— CLB → CLB, CLB → RED are the same as CLB → CLA and CLB → P700.
— CAR → CLB, CAR → RED are the same as CAR → CLA and CAR → P700.

In table 2, we resume the different R_0 values with references.

We located the red form chlorophylls corresponding to the A5 and B5 positions of each lhca of the PSI complex in the 5L8R PDB (using the naming convention proposed by Kühlbrandt [51]) as these positions were suggested to be associated with red-shifted absorption spectra by Morosinotto *et al.* [52,53]. To give an example, we depict the red form chlorophyll A5 and B5 of the lhca2 in electronic supplementary material, appendix, figure SA1.

2.3. The cut-off distance

The links in the PSI network are associated with different FRET efficiencies as a function of the nodes' pairwise distance in the PDB structure. The closer the nodes, the higher the link weight (FRET efficiency) joining them. We defined the cut-off distance (CD) as the distance between two nodes over which we assume the link between them absent because the associated FRET efficiency computed by equation (2.1) is too low. By lowering the CD parameter, we keep only those links with lower associated pairwise distance (and higher FRET efficiency) between the nodes. Using this parameter, we can build different networks from the original PSI network with different number of links as a function of their FRET magnitude. In other terms, starting from the network where all possible links are drawn, when lowering the CD, we operate a removal of the links of higher distance (lower weight) maintaining the links of shorter distance (higher weight). We created 10 networks using the following CD values: NO cut-off, 90, 80, 70, 60, 50, 40, 30, 20 and 10 Å.

2.4. Measures of network functioning

2.4.1. The largest connected component

The largest connected component (LCC) is a widely used measure of the network functioning [22,50,54]. The LCC is also known as

Table 2. R_0 among the different types of nodes/chromophores with references.

from	to	R_0 (Å)	reference
CLA	CLA	90	[45,46]
CLA	CLB	5	[50]
CLA	RED	90	as CLA → CLA [45,46]
CLA	P700	90	[45,46]
CLB	CLA	100	[47]
CLB	CLB	100	as CLB → CLA [47]
CLB	RED	100	as CLB → CLA [47]
CLB	P700	100	[47]
RED	CLA	10	[49]
RED	RED	90	as CLA → CLA [45,46]
RED	P700	10	[49]
CAR	CLA	21.7	[48]
CAR	CLB	21.7	as CAR → CLA [48]
CAR	RED	21.7	as CAR → CLA [48]
CAR	P700	21.7	[48]

giant component and it accounts for the highest number of connected nodes in the network. We compute two types of LCC, by considering the weakly largest connected component (LCC_{weak}) and strongly largest connected component (LCC_{strong}). The LCC_{weak} represents the largest number of nodes in the network in which every node can reach any other by an undirected path. Differently, the LCC_{strong} represents the largest number of nodes in which every node can reach any other node by a directed path [31].

2.4.2. Network efficiency

Eff is a widely used measure of network functioning evaluating how efficiently the network exchanges information [24,55,56]. Eff is based on the shortest paths (SP) notion. A path is a sequence of links connecting two nodes in the network; a binary shortest path between a pair of nodes is the minimum number of links that we have to pass travelling between the nodes [57]. Differently, the weighted shortest paths (wSP) consider both the number of links and the weight attached to them. To calculate wSP, we first compute the inverse of the link weights; then we compute the wSP as the minimum sum of the inverse link weights necessary to travel among nodes [31,38].

The average efficiency of the network is then defined:

$$\mathrm{Eff} = \frac{1}{N \cdot (N-1)} \sum_{i \neq j \in G} \frac{1}{d(i,j)}, \tag{2.2}$$

where $d_{i,j}$ is the shortest path between node i and node j, the longer the SP among nodes, the lower the efficiency of the network. The efficiency can be computed for undirected and directed networks when considering undirected and directed SP, respectively. Furthermore, the Eff can properly evaluate binary and weighted networks; in the case, network is weighted, $d_{i,j}$ indicates the weighted shortest path between nodes i and j. Since the PSI is a weighted and directed network, we used the weighted and directed Eff.

2.4.3. The number of connected nodes to P700

CN signifies the number of connected nodes to P700 through a path. This new measure we introduce here indicates how many nodes in the network can actually transfer energy to the P700 RC. The energy can flow from the node to P700 directly (through one link) or indirectly (the energy flows to P700 in many steps, i.e. passing over different nodes). In other words, CN accounts the number of nodes/chromophores that can properly contribute to PSI functioning. For comparison, the number of nodes directly connected (one link) to P700 is computed (1-step paths to P700).

2.5. The PSI network properties

We analysed the PSI system using well-known notions from networks science. Node degree (k) is the total number of links to the nodes [31]. We also computed number of ingoing links, i.e. the in-degree (k_{in}) and the number of outgoing links, the out-degree (k_{out}). Node strength (S) is the sum of the link weights to the nodes [56]. The strength of a node is the weighted counterpart of the node degree (k). Analogously, we can compute the ingoing strength (S_{in}) and the outgoing strength (S_{out}). Node betweenness centrality (BC) is a widely used measure of nodes centrality based on SP. The BC of a node is the number of the SP between all nodes pairs that pass through that node [31,58]. Here, we adopt both the binary BC and the weighted version of the BC of the nodes (BCw). The BCw is computed using the wSP. The BCw of a node accounts the number of wSP from any couple of nodes passing along that node. The higher is the BCw of a node, the higher is the number of wSP passing along it (and the more central is the node). δ centrality: the node δ centrality signifies the decrease of the Eff triggered by the removal of that node from the network [55]. The higher the δ, the higher the contribution of the node on the Eff.

2.6. The nodes removal simulations

We simulated different node removal (attack) processes over the PSI network [22,33,59]. Removal of nodes from the PSI network may describe functionality loss of the chromophores, which can be due by ageing, disease, pollution or others [3]. The node removal processes (strategies) can be divided in two main classes. The first is the selective removal of a certain type of node/chromophore, that is an attack towards specific PSI nodes. Thus, selective node removal of the LHCI randomly removes nodes only from the LHCI ensemble that is composed of 68 nodes; the selective node removal of Chls randomly removes nodes from the Chls (156 nodes); for the CAR, we randomly removed only carotenoids nodes (36 nodes) and so on. Then for each selective removal, we performed the control experiment by randomly removing the same number of nodes from the entire network (for example, the Rand Control for the CAR removed 36 nodes from the whole network). Control node removal represents the benchmark comparison for the harm to the PSI network triggered by the selective node removal strategies.

We measured the functioning of the network during the node removal process using the Eff (figure 3*c*) and the LCC_{weak}. Since the random removals are stochastic processes, we average the outcomes from 10^3 simulations. The average damage triggered in the system by the selective PSI nodes removal (CAR, Chls, LHCI, etc.) is then compared with the average damage induced by the random removal (Control) of the same number of nodes. In this way, we can discriminate the importance of the different types of nodes/chromophores.

2.7. The robustness of the network

When nodes are removed from the network, the PSI system loses nodes/chromophores and the EET paths passing on them, with a consequent system functioning decrease (figure 3*a*,*b*). We can assess the system damage resulting from node removal according to the functioning measures. The more important the nodes

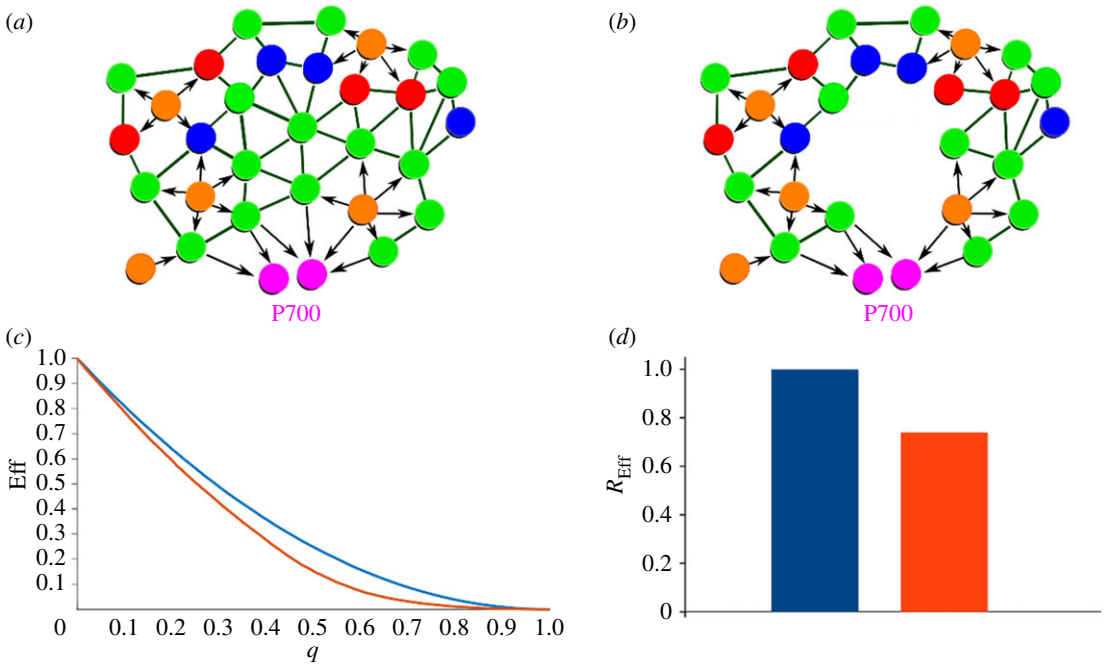

Figure 3. (*a*) Example network where nodes/chromophores perform EET towards the RC; (*b*) this network represents the network (*a*) after the removal of three green nodes (CLA), where we can see the elongation and the disruption of the EET paths and the consequent network functioning decrease; (*c*) functioning efficiency measure (Eff) as a function of the fraction of nodes removed (*q*) for two hypothetical different attack strategies; the red strategy triggers a faster efficiency (Eff) decrease than the blue strategy and the network robustness area below the red curve is lower than the one below the blue curve. (*d*) The robustness (R_{Eff}) of the efficiency computed for the two strategies. The bar robustness R_{Eff} corresponds to the area below the curve in the left chart (*c*); R_{Eff} value is normalized by the max value, e.g. by R_{Eff} of the blue strategy.

removed from the network, the steeper the decrease in the network functioning measure. For example, in figure 3*c*, the red removal strategy identifies more important nodes causing a steeper decrease in the Eff with respect to the blue strategy. To compare the response among node removal strategies, we resumed the outcome in a single value defined network robustness (R), depicted by the bar plots of figure 3*d*. The value of R corresponds to the area below the curve of the system functioning measure subjected to node removal. We referred to R_{Eff} and R_{LCC} when the network functioning is evaluated by the Eff and LCC, respectively. All the calculations have been performed using Matlab (2019b) and R (v. 4.0.2). The biological images of the PSI were created using Pymol software (v. 2.4.0).

3. Results

3.1. The network properties

In table 3, we resume the PSI network properties for each CD value. The number of links L, average nodes degree $\langle k \rangle$ and average nodes strength $\langle S \rangle$ linearly decrease lowering CD (figure 4). The nodes degree k ranges in the interval $0 < k < 307$. The nodes degree distribution is a two values distribution with $k = 307$ as the most frequent value for NO CD, a bell-shaped distribution of decreasing mean from CD = 90 Å to CD = 20 Å, a Poisson-like distribution with most of the values approaching the $k = 0$ for CD = 10 Å (electronic supplementary material, appendix, figure SA2). The node strength distribution follows the node degree distribution patterns indicating a node's degree/strength coupling (electronic supplementary material, figure SA3). The average link weight Ew shows a slow increase lowering CD (figure 4); the link weight distributions are skewed to the left with many links presenting weight 1 and a few links of lower weight (electronic supplementary material, figure A4). The Eff remains roughly constant by decreasing CD from NO CD to CD = 70 Å; after this value, we find a more pronounced Eff decrease reaching the minimum for CD = 10 Å (figure 4). LCC_{weak} spans the whole network with $N = 192$ nodes up to reach CD = 20 Å (figure 4). LCC_{strong} holds the values $N = 154$ up to reach CD = 20 Å (figure 4). Investigating the PSI network properties for CD < 20 with finer-grained tuning, we find that the critical threshold to have the LCC_{weak} and LCC_{strong} collapse is CD = 14 Å and below this value, the LCCs quickly drop to quasi-zero (electronic supplementary material, figures SA5 and SA6). We find 192 nodes connected to the P700 (CN) and this number holds constant up to reach CD = 20 Å (figure 4). Only for CD = 14 Å, CN quickly drops to zero (electronic supplementary material, figure A7). It is worth noting that for LCC_{weak}, LCC_{strong} and CN measures, the critical CD value is 14 Å, below which the measures quickly collapse. Differently, we find that the number of 1-step paths to P700 follow a more linear and faster decrease even as CD = 80 Å (figures 4 and 7).

3.2. The properties and connectivity of the different nodes/chromophores

The Chls show the highest degree and out-degree (figure 5, panels k and k_{out}), BC (figure 5, panels BC and BCw), strength and out-strength (figure 5, panels S and S_{out}) and δ centrality than all the others types of nodes/chromophores; P700 has the highest in-degree (panels K_{in}) and in-strength (panels S_{in}) (figure 5); the LHCI values are found ranging between the Core and the P700 for most of the analysed node properties (figure 5). Chls show the highest degree and in-degree (figure 5, panels k and k_{in}), BC (figure 5, panels BC and BCw), strength (figure 5, panels S and S_{in}) and δ centrality than all the other types of nodes/chromophores (figures 5 and 6). More

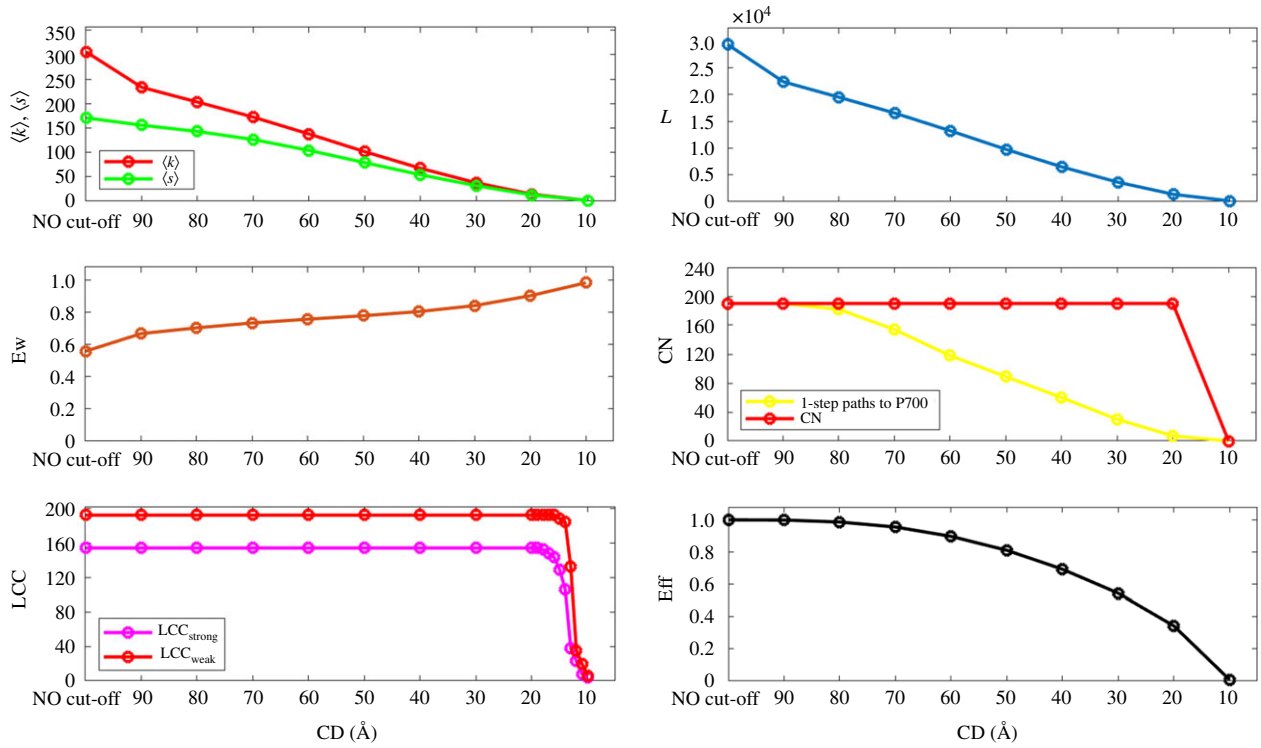

Figure 4. Network properties as a function of CD. Average nodes degree $\langle k \rangle$ and average nodes strength, number of links L, average link weight Ew, CN number of connected nodes to the P700 and number of 1-step paths to P700, largest connected component LCC (weak and strong); network efficiency Eff.

Table 3. PSI network features for each CD value. $\langle k_{in} \rangle$, average nodes in-degree; $\langle k_{out} \rangle$, average nodes out-degree; $\langle k \rangle$, average nodes degree; $\langle S_{in} \rangle$, average in-strength; $\langle S_{out} \rangle$, average out-strength; $\langle S \rangle$, average node strength; L, total number of links; LCC_{strong}, strongly largest connected component; LCC_{weak}, weakly largest connected component; Eff, global network efficiency; Ew, average link weights; CN to P700, number of connected nodes to the P700; *1-step paths to P700*, number of 1-step paths from any node to P700.

CD	$\langle k_{in} \rangle$	$\langle k_{out} \rangle$	$\langle k \rangle$	$\langle S_{in} \rangle$	$\langle S_{out} \rangle$	$\langle S \rangle$	L	LCC_{strong}	LCC_{weak}	Eff	Ew	CN to P700	1-step paths to P700
10 Å	0.74	0.74	1	0.73	0.73	1.45	142	4	6	0	0.98	0	0
20 Å	7.06	7.06	14.11	6.37	6.37	12.74	1355	154	192	0.18	0.9	190	7
30 Å	18.86	18.86	37.72	15.86	15.86	31.72	3621	154	192	0.29	0.84	190	30
40 Å	33.7	33.7	67.41	27.11	27.11	54.21	6471	154	192	0.37	0.8	190	60
50 Å	50.74	50.74	101.48	39.5	39.5	79	9742	154	192	0.43	0.78	190	89
60 Å	68.85	68.85	137.7	52.11	52.11	104.23	13219	154	192	0.48	0.76	190	118
70 Å	86.16	86.16	172.31	63.19	63.19	126.38	16542	154	192	0.51	0.73	190	154
80 Å	101.58	101.58	203.17	71.44	71.44	142.88	19504	154	192	0.53	0.7	190	182
90 Å	116.67	116.67	233.34	77.86	77.86	155.73	22401	154	192	0.53	0.67	190	190
NO CD	153.07	153.07	306.15	85.41	85.41	170.81	29390	154	192	0.53	0.56	190	190

specifically, the Chla nodes present the highest BC, S and δ centrality than all the other types of nodes/chromophores and other types of Chls. CARs show the highest out-degree (figure 5, panel k_{out}), similar to the Chls nodes. Considering the connectivity between different subunits of the PSI, we find a higher number of intra-Core links (greater than 11 000) than LHCI-Core links (approx. 6500) for CD = NO and this advantage holds for all CDs (figure 7*b*); conversely, we find a lower number of intra-LHCI links (approx. 4000) than LHCI-Core links (approx. 6500) for CD > 60 Å, whereas for CD < 60 Å, the pattern is opposite and the number of intra-LHCI links becomes higher (figure 7*b*); we find that the Core shares 120 directed paths (1 directed link) to the P700 for CD = NO and this number remains roughly constant up to reach CD = 60 Å, and after this value shows a slow decrease (figure 7*a*); we find that the LHCI has approximately 65 directed paths to the P700 for CD = N0 with a faster decrease for CD > 80 Å (figure 7*a*).

3.3. Nodes removal

3.3.1. Carotenoids

Rand CAR induces less average damage to the Eff (higher R_{Eff}) of the PSI network than the random removal control (Rand)

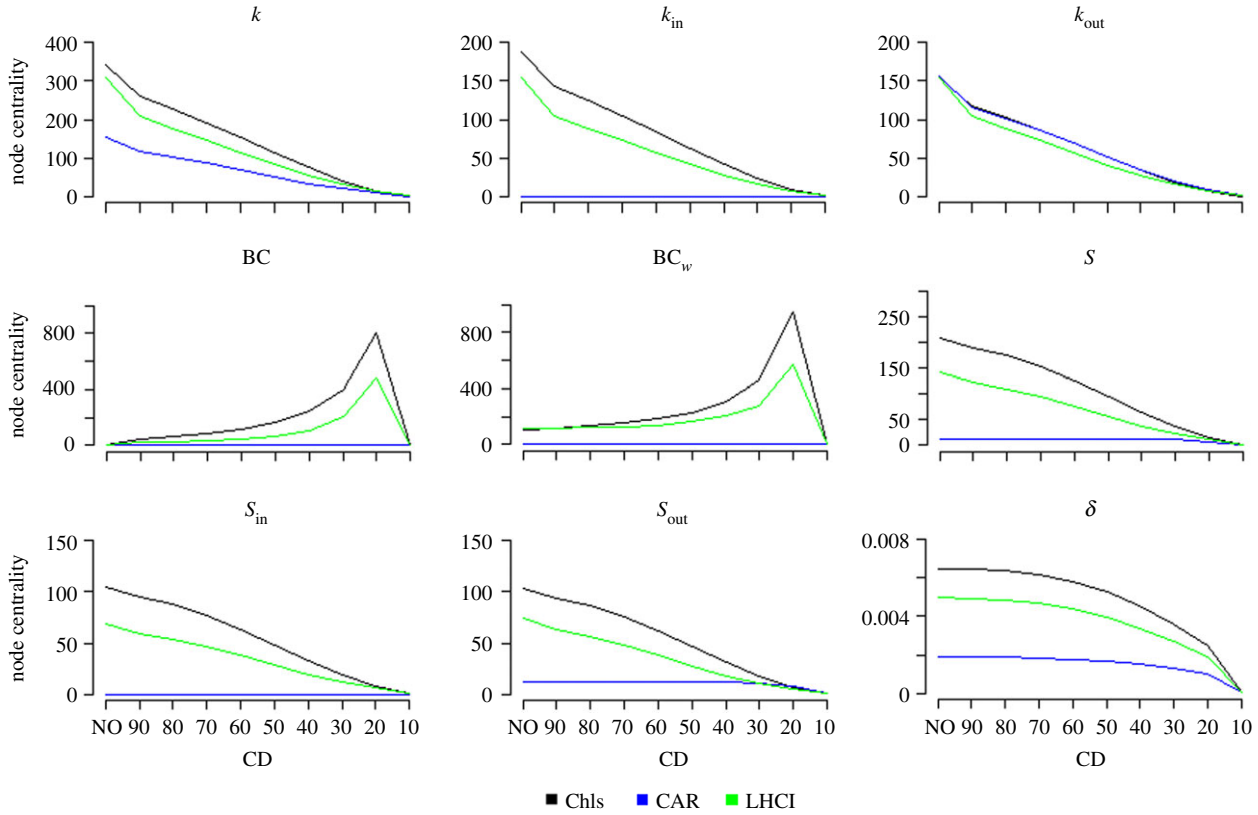

Figure 5. Node centrality features for the different types of PSI network nodes as a function of the CD. Node centralities keys are: k degree of the nodes, k_{out} out-degree, k_{in} in-degree; BC binary betweeness centrality; BC_w weighted betweeness centrality; S node strength, S_{in} ingoing node strength, S_{out} outgoing node strength; δ decrease in the directed network efficiency after single node removal. Node type: Chls, chlorophylls; CAR, carotenoids; LHCI, light-harvesting complex I.

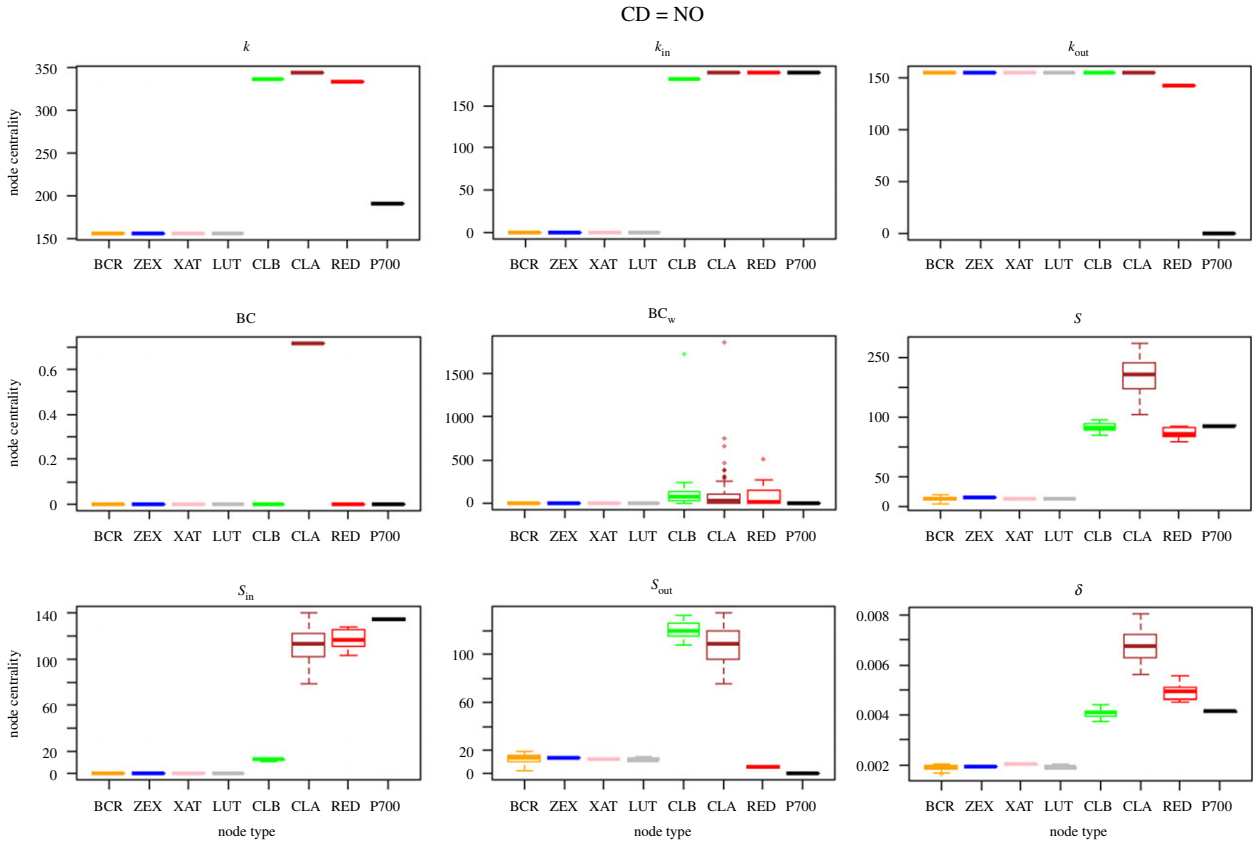

Figure 6. Boxplots of node types versus nodes centrality feature for the PSI network features for NO cut-off (CD = NO). Node properties keys are: k degree of the nodes, k_{out} out-degree, k_{in} in-degree; BC binary betweeness centrality; BC_w weighted betweeness centrality; S node strength, S_{in} ingoing node strength, S_{out} outgoing node strength; δ decrease in the directed network efficiency after single node removal. Node types keys are: β-carotene BCR, β-carotene derivated ZEX, violaxanthin XAT, lutein LUT, chlorophyll *b* CLB, chlorophyll *a* CLA, red form Chls RED, PSI reaction centre P700.

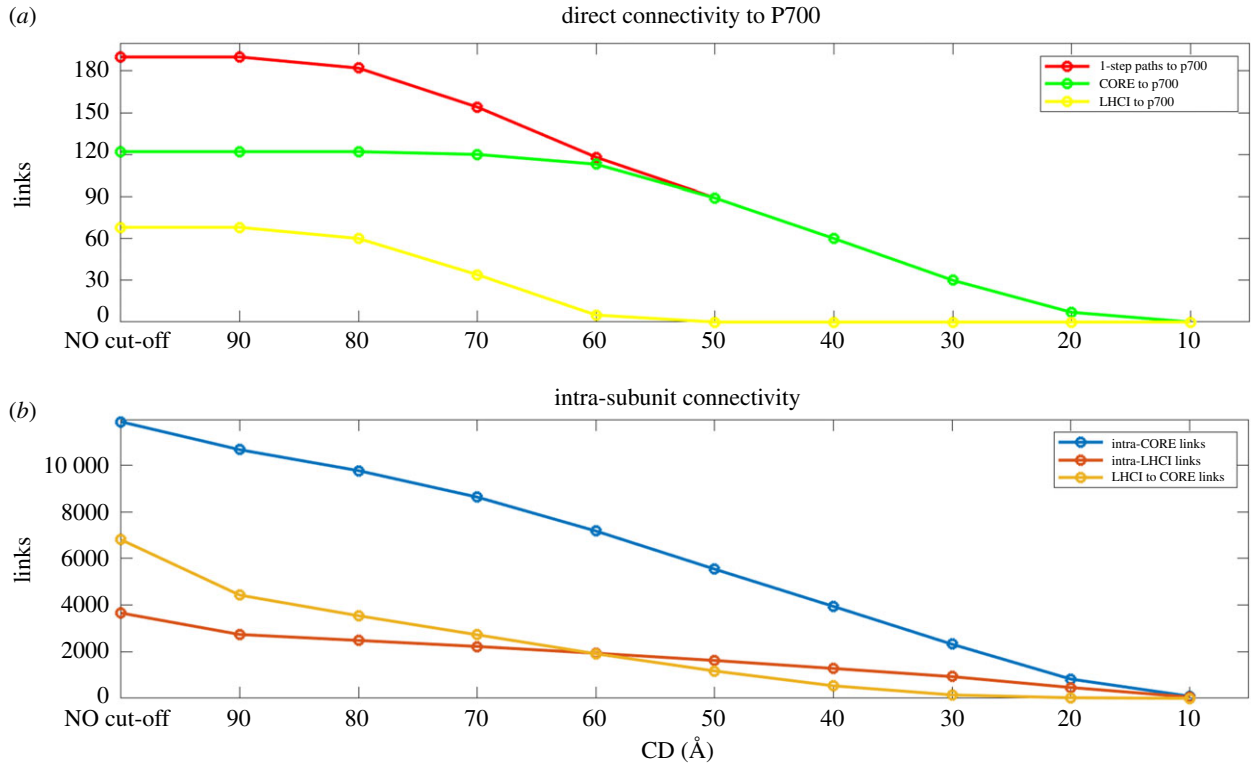

Figure 7. Number of links among different types of nodes/chromophores as function of CD. (*a*) Number of links between CORE nodes and P700 nodes (green line) and between LHCI nodes and P700 (yellow line), compared to the number of 1-step paths to P700 of all nodes (red line, reported in figure 4). We observe that CORE nodes are more connected to the P700 than LHCI nodes throughout all CDs. (*b*) Number of links between nodes of the same subunit: CORE (blue line), LHCI (red lines) compared to the number of links between LHCI nodes to CORE nodes (yellow line). We see that the number of links between LHCI-CORE is greater than the number of intra-LHCI links until 60 Å.

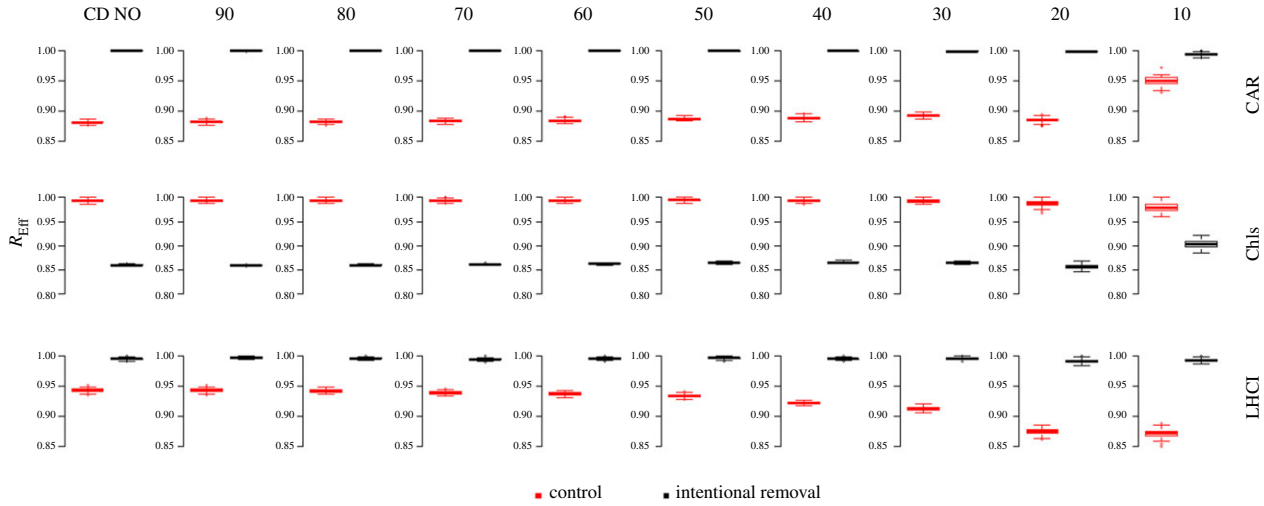

Figure 8. Boxplots of the PSI network robustness (R_{Eff}) under the random removal (Control) and the intentional random nodes removal (Intentional removal) strategies for the different CD, for the three macro types of nodes/chromophores: LHCI (all nodes/chromophores found in the LHCI of the PSI), Chls (all chlorophylls) and CAR (all types of carotenoid molecules).

(figure 8). The Rand CAR shows roughly 15% fewer R_{Eff} than Rand. This difference between the R_{Eff} values decreases by lowering CD. The lower damage triggered by CARs holds with various differences even when investigating each type of carotenoid node individually (figure 10). We find that the highest difference is between intentional removal and the control for the β-carotene nodes (BCR). Differently, when measuring the robustness with the R_{LCC}, Rand CAR induces the same average damage to the LCC_{weak} than Rand (electronic supplementary material, figure A22). Only for CD = 10 Å do we find a difference between the R_{LCC} values of Rand CAR and Rand, with Rand CAR triggering higher damage than the control Rand (electronic supplementary material, figure SA22).

3.3.2. Light-harvesting complexes I

Random removal of LHCI (Rand LHCI) causes less damage to Eff (higher R_{Eff}) than the random removal control (Rand) for all CDs (figure 8) and for each LHC when analysed individually (electronic supplementary material, figure A21).

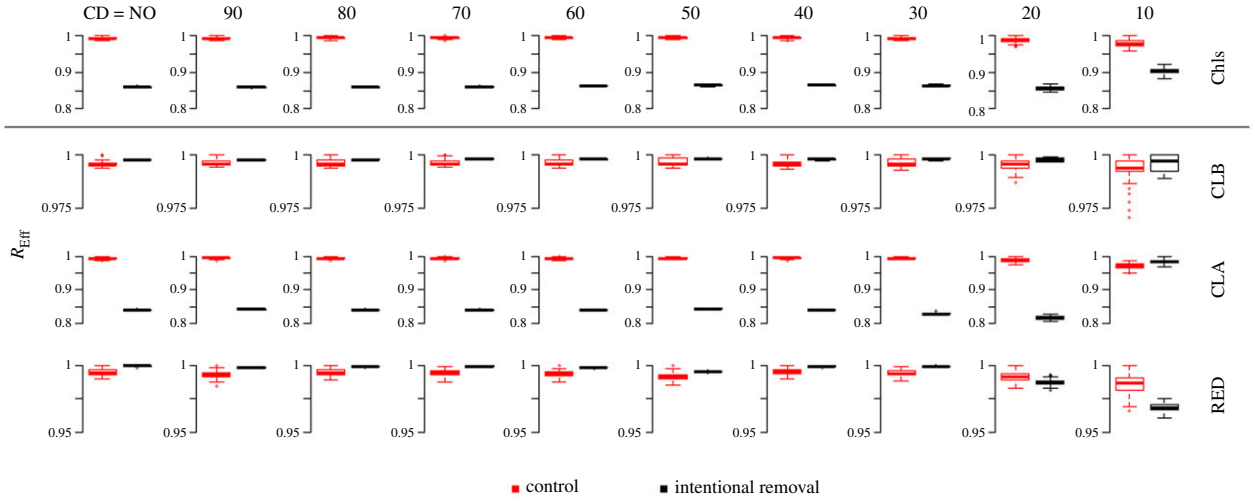

Figure 9. Boxplots of the PSI network robustness (R_{Eff}) under the random removal (Control) and the intentional random nodes removal strategies towards the Chls nodes/chromophores for the different CD. Rows indicate the removal towards Chls (all chlorophyll types), CLB (chlorophyll *b*), CLA (chlorophyll *a*) and RED nodes (red form chlorophylls).

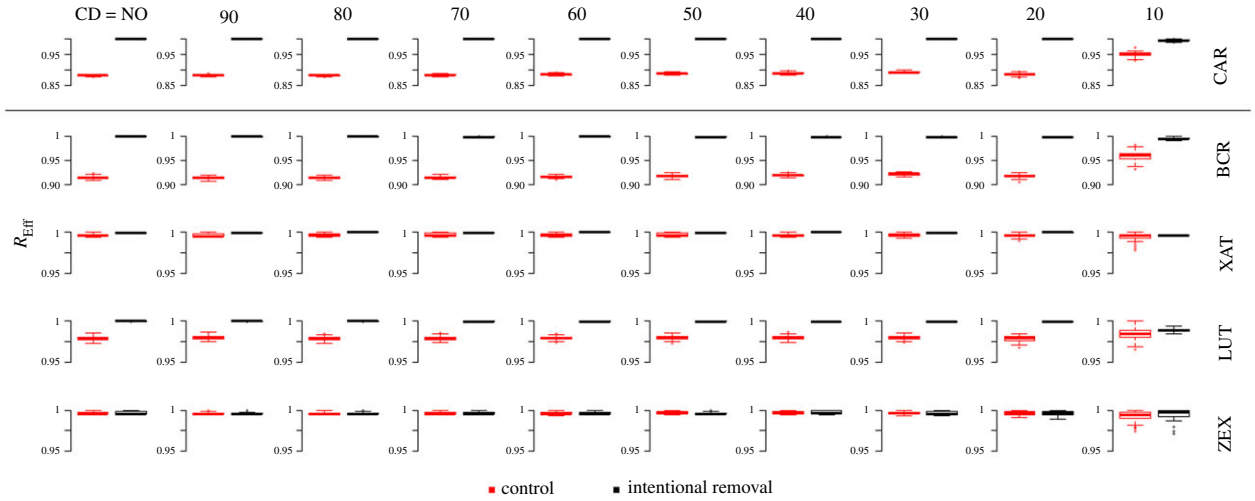

Figure 10. Boxplots of the PSI network robustness (R_{Eff}) under the random removal (Control) and the intentional random nodes removal strategies towards the carotenoids nodes/chromophores for the different CDs. Rows indicate the removal towards CAR (all types of carotenoid molecules), BCR (β-carotene), ZEX (β-carotene derivate), XAT (violaxanthin), LUT (lutein).

Differently, the Rand LHCI induces slightly higher average damage to the LCC_{weak} (higher R_{LCC}) than Rand for all CDs except for CD = 10 Å (electronic supplementary material, figure SA22). Even when analysing each lhca individually, the Rand LHCI induces slightly higher average damage to the LCC_{weak} (higher R_{LCC}) than Rand for all CDs, except for lhca3 (electronic supplementary material, figure SA23).

3.3.3. Chlorophylls

Random removal of Chls (Rand Chls) causes more damage to Eff (lower R_{Eff}) than the random removal control (Rand) (figure 8). The R_{Eff} obtained by Rand Chls is *ca* 15% lower than that induced by the Rand. When analysed individually, we find that the Rand chlorophyll *a* triggers higher damage to Eff than the control except for CD = 10 Å (figure 9), whereas for the other Chls type, i.e. chlorophylls *b* and red forms, the pattern is opposite and the intentional removals (Rand CLB and Rand RED) trigger lower damage to Eff than the control (Rand). Rand Chls causes more damage to LCC_{weak} than the control Rand (electronic supplementary material, figure SA22). This difference is less pronounced for CD = 10 Å. We find that for the Chls type analysed individually, the intentional removal triggers the same damage to the LCC_{weak} with respect to the control Rand; only removal of chlorophyll *a* (Rand CLA) triggers highest damage to the LCC_{weak} than the control Rand for CD < 30 Å (electronic supplementary material, figure SA24).

4. Discussion

4.1. Network properties

The Chls nodes show the highest degree (k and k_{out}) among all other types of chromophores, i.e. they share the highest number of links in the network (figures 5 and 6). This indicates that the Chls of the PSI network are the major components in the global energy transfer and it is confirmed by their highest BC for all CDs (figures 5 and 6). In particular, the chlorophyll *a* nodes (CLA) show the highest BC (both

BC and BCw) among Chls. The nodes with highest betweenness are the articulation points routing the shortest and the most efficient energy transfer paths in the network [31]. As a consequence, these findings demonstrate that the Chls (and especially the chlorophyll *a* nodes) are the 'highest connected' and 'most central' components in the PSI network of the *P. sativum*, corroborating previous outcomes from the literature showing that the primary function of the Chls is to enhance the EET efficiency in the system [4,5].

Furthermore, chlorophyll *a* nodes have the highest node strength *S* value, followed by chlorophyll *b* nodes and red form Chls, both almost at the same level (figure 6). The strength (*S*) is the sum of the link weights to the node, and to present higher *S* indicates that the CLA nodes share many links of higher FRET efficiency. Then, regarding the directionality of the link weights, we observe that chlorophyll *b* nodes have the highest S_{out}, the red form Chls have the highest S_{in}, while CLA nodes have intermediate values in both measures. Even these findings suggest that chlorophylls *a* are the most central chromophores playing the important role of articulation points of the EET process in PSI. On the other hand, chlorophylls *b* nodes (CLB), showing higher outgoing link weights (S_{out}), would play the role of important EET outgoing energy transfer spreaders towards other chromophores, similarly to the role played by CAR nodes. While both chlorophylls *b* and carotenes transfer energy within the PSI [60], these outcomes, from a network science viewpoint, would show that the primary function for these chromophores is not being central and pivotal nodes for the EET in the PSI of the *P. sativum*. Differently, the red form Chls (RED) show highest S_{in}, indicating the higher EET towards these nodes, and almost zero S_{out}, showing *quasi*-zero EET flowing out of the red form chlorophylls (figure 6). These outcomes would describe the red form Chls as important energy transfer receivers with negligible activity in transfer energy towards other nodes/chromophores, and noteworthy, they corroborate the hypothesis indicating the red-shifted Chls as energetic wells in the EET mechanisms of the PSI system, with a role in slowing down of the EET process [12,61]. For this reason, we support the hypothesis that the red form Chls primary function would be different from chlorophyll *a*, e.g. to increase the absorption of longer wavelength and widen the light harvested spectrum of PSI [62]. We outline that these discoveries focusing on the relationship between function and the topological role of the different chromophores in PSI, even carried out with our seminal network model of PSI, recover the main results regarding chromophore function from the literature [63].

4.2. Feasibility of the PSI EET

When lowering the CD, nodes require a shorter pairwise distance to perform FRET. In other terms, when lowering the CD, we progressively remove the weak links of lower FRET efficiency from the network and keep only the most efficient and most probable ones (strong links). The strong links connecting chromophores at the lowest CD values can be viewed as the most 'feasible FRET' energy transfer, i.e. the energy transfer links with higher likelihood to occur. We discover that lowering the CD, the number of energy transfer links (*L*) in the PSI linearly decreases (figure 4). The loss of links among nodes causes both the loss and the elongation of the EET paths within the PSI network and the consequent decrease in its Eff (figure 4). Hence, when lowering the CD, the PSI system experiences a reduction in the Eff, while the maximum number of connected nodes/chromophores LCC holds constant down to CD = 14 Å. Also, the number of nodes connected by paths to the P700 RC (CN) holds constant down to CD = 14 Å. This indicates that only for CD = 14 Å, the links are not enough to connect the nodes, the network nodes lose many energy transfer paths and the nodes/chromophores are unable to perform the energy transfer to the RC, thus impairing PSI functioning. These outcomes give us information about the whole feasibility of the PSI EET functioning, showing that the Eff is negatively affected by lowering CD; even so, the possibility to perform FRET in the whole network is severely impaired only reaching the lowest values of CD. The FRET appears to have played the role of a design constraint shaping the evolution of photosynthetic organisms and had profound influence in shaping their architecture [44,45,64]. Our model can shed light on the structural evolution of the PSI, showing how the PSI network formed by FRET links is a very resilient system with a large 'window of feasibility', holding the capacity to perform the energy transfer in the whole network even when deprived of the most of FRET links.

4.3. Connectivity among different PSI subunits

When analysing the connectivity among different subunits of the PSI complex network, we find a far greater number of intra-CORE links connecting the nodes/chromophores belonging to the CORE showing how spatially closer are the nodes in the CORE with respect to other subunits (figure 7). Furthermore, we find that for higher CD values, there is a higher LHCI-CORE linkage density than intra-LHCI. Only decreasing CD below to CD = 60 Å, the intra-LHCI and the LHCI-CORE links densities become comparable, and for CD = 60 Å, the network is formed by FRET links shared in similar number in LHCI-CORE and intra-LHCI links (figure 7). These findings show that lowering the CD produces a faster decrease in the LHCI-CORE links with small effect in decreasing the intra-LHCI links. On the one hand, this indicates that LHCI are spatially closer among them than they are with the CORE Chls. On the other hand, this shows that the intra-LHCI links are stronger links of higher FRET whereas a significant amount of LHCI-CORE connections are weaker links of lower FRET efficiency.

It is arguable that the more the FRET links perform energy transfer in the PSI network, the higher the PSI system functioning level. In the case only the strong links among closest chromophores (i.e. CD < 60 Å) are performing the energy transfer, the PSI system should be in a lower level of functioning with respect to the case of all the FRET links (also the weaker links) performing energy transfer. For these reasons, we can call these stronger, higher probable links held in the network for lower CD values (CD < 60 Å) the 'low functioning regime links', to indicate that they would be the only active energy transfer links when the PSI is at lower level of functioning. Conversely, when tuning higher CD (CD > 60 Å), we keep lower FRET efficiency links that we can consider working together with the strong links when the PSI is at higher level of functioning. We call these weaker FRET links for CD > 60 Å, the 'high functioning regime links', thus denoting that they would be active and feasible energy transfers when the PSI system is at higher level of functioning. Following the above distinction of the PSI links, our findings would describe a PSI system

composed by higher probable intra-LCHI links (CD < 60 Å), that we hypothesize are the 'low functioning regime links' when the PSI is at lower level of functioning, and a large amount of weaker, less probable LHCI-CORE links, i.e. the 'high functioning regime links' (CD > 60 Å) that we may argue to be active when the system is at higher level of functioning.

4.4. The nodes/chromophores attack

The aim of the node removal (attack) strategy simulations was to mimic the loss of functionality of the chromophores of the PSI network, giving us information on how different network nodes/chromophores contribute to the functioning efficiency of the overall system [2,3]. In normal conditions when chromophores lose their functionality, they are readily substituted in the turnover process [65,66]. In the case the turnover machinery is impaired, the system loses chromophores making the photosystem functionality deteriorate progressively. The decrease in the number of chromophores in photosynthesizing organisms may be the result of genetic mutations, chemical damage, pollution [67] and the changing environment of the chromophores [3]. The reduction in Chls number (or functionality) can also be associated with natural phenomena as the yellowing of senescing leaves and autumnal colour changes in the foliage of deciduous trees, but also in seeming evergreens, such as ferns and algae [68] and leaf ageing [65].

Removing a node/chromophore in the PSI network would affect the system in two ways. On the one hand, it removes one entry gate for light from the system, thus lowering the light-harvesting capacity. On the other hand, it removes all the links relating to that node/chromophore breaking up the paths for the FRET passing into that node. Path disruption triggers both the lengthening of the energy transfer distance and the decrease in the number of the EET paths among nodes; the combination of these effects triggers a decrease in the Eff (figure 3).

We observed that the removal of nodes corresponding to carotenoid molecules (CAR) induces lower average damage to the network functioning (Eff and LCC) than the control random nodes removal (figure 8). In fact, CAR are nodes possessing only outgoing links and have the lowest BC, not playing the role of halfway hubs for the FRET paths in the network. Thus, their removal will not induce a significant FRET paths disruption, resulting in a lower network efficiency decrease. This outlines the importance of small carotenoids for the structural efficiency of the EET, and relegating their main role for other important functions, as broadening the spectrum of absorbable light and photo-protection [5].

Similarly, we find that random removal of nodes belonging to LHCI causes lower average damage to network functioning (Eff) than the random control (figure 8). As for carotenoids, LHCI nodes show low BC (figure 5), indicating their minor role for routing the SP in the network and consequently the lower damage to the PSI Eff caused by their removal. For this reason, we argue that LHCI plays a major role in increasing the PSI absorption cross-section as proposed by the authors in [63,69] but not in the efficiency of the EET of the PSI, that is mainly given by the CORE.

Differently, we find that the random removal of Chls triggers the greatest decrease in the network functioning (Eff and LCC) (figure 8; electronic supplementary material, figure SA22) and the single removal of Chls triggers the highest decrease in Eff than all the other types of nodes (δ indicator in figures 5 and 6). Further, when discriminating the damage induced by each different type of Chls, we find that chlorophyll *a* causes the highest decrease in the PSI network functioning efficiency (CLA row, figures 9 and 10). To note, chlorophyll *a* induces clearly higher damage even than the other Chls type, i.e. chlorophyll *b* and red form Chls. The higher damage to the system EET induced by the removal of chlorophyll *a* may be explained with their peculiar embedding within the structure of the PSI network. Chlorophyll *a* shows the highest node BC, i.e. these nodes are crucial articulation points for the FRET SP among the network nodes (CLA, figure 6). Their removal breaks up many higher efficiency FRET paths causing greater damage to global energy transfer measured by the Eff, raising chlorophyll *a* as the key network component directly involved in the increase in EET of the *P. sativum* PSI, confirming by means of network theory previous results from experimental analysis [63,70,71].

5. Conclusion

In this paper, we modelled the PSI of the *P. sativum* as a complex interacting network. First, we discovered that progressively removing the weaker FRET links decreases the Eff, while the node connectivity is still preserved. This finding would unveil a large window of feasibility of PSI functioning, in which the photosynthetic process is completely impaired only losing almost all the links in the network. In other terms, the PSI networked system would be highly resilient to the malfunctioning of FRET links. Second, we discovered that chlorophyll *a* removal triggers the fastest functioning decrease, indicating these chromophores of the PSI network as the main actor boosting the EET. Since the nodes removal simulates the chromophores malfunctioning, caused, for example, by the senescing leaves, biological diseases, pollution, chemical damage or others [68], the PSI energy transfer efficiency would be more vulnerable to chlorophyll *a* functionality loss. For these reasons, considering all types of chromophores of the PSI, the use of network science presented here shows that chlorophyll *a* is the key contributor to the EET efficiency, while other chromophores (chlorophyll *b* and carotenoid molecules) have different primary functions. The coherence of these results with the literature and the new insights on the PSI EET structure justifies the use of network theory to study photosynthetic systems, even with approximated, non-quantum models. The outcomes presented here open promising new areas of research, for example, building and comparing the energy transfer efficiency of the PSI network of different natural and agricultural plant species, or improving the light-harvesting mechanisms of artificial photosynthesis both in plant agriculture [70,71] and in the field of solar energy applications [72].

Data accessibility. This article has no additional data.

Authors' contributions. D.M. and M.B. conceived, performed the analyses and wrote the paper. D.C., F.S. and A.M.R. wrote the paper.

Competing interests. We declare we have no competing interests.

Funding. M.B. and F.S. acknowledge financial support from Fondazione Cariplo, grant no. 2018-0979. This project has received funding from the European Research Council (ERC) under the European Union's Horizon 2020 research and innovation programme (grant agreement no. [816313]).

Acknowledgements. The authors are grateful to two anonymous reviewers whose suggestions greatly improved the manuscript. We thank Prof. Guglielmo Lanzani for his suggestions on the first version of the manuscript.

References

1. Michael NDC. 2017 20.1 Photosynthetic carbohydrate synthesis. In *Lehningner principles of biochemistry* (eds DL Nelson, M Cox), 7th edn, pp. 756–763. New York, NY: WH Freeman.
2. Baker LA, Habershon S. 2015 Robustness, efficiency, and optimality in the Fenna–Matthews–Olson photosynthetic pigment–protein complex. *J. Chem. Phys.* **143**, 105101. (doi:10.1063/1.4930110)
3. Baker LA, Habershon S. 2017 Photosynthetic pigment–protein complexes as highly connected networks: implications for robust energy transport. *Proc. R. Soc. A* **473**, 20170112. (doi:10.1098/rspa.2017.0112)
4. Mazor Y, Borovikova A, Caspy I, Nelson N. 2017 Structure of the plant photosystem I supercomplex at 2.6 Å resolution. *Nat. Plants* **3**, 17014. (doi:10.1038/nplants.2017.14)
5. Mirkovic T, Ostroumov EE, Anna JM, Van Grondelle R, Govindjee SGD. 2017 Light absorption and energy transfer in the antenna complexes of photosynthetic organisms. *Chem. Rev.* **117**, 249–293. (doi:10.1021/acs.chemrev.6b00002)
6. Fromme P, Jordan P, Krauß N. 2001 Structure of photosystem I. *Biochim. Biophys. Acta Bioenergy* **1507**, 5–31. (doi:10.1016/S0005-2728(01)00195-5)
7. Shen J-R. 2015 The structure of photosystem II and the mechanism of water oxidation in photosynthesis. *Annu. Rev. Plant Biol.* **66**, 23–48. (doi:10.1146/annurev-arplant-050312-120129)
8. Busch A, Hippler M. 2011 The structure and function of eukaryotic photosystem I. *Biochim. Biophys. Acta Bioenergy* **1807**, 864–877. (doi:10.1016/j.bbabio.2010.09.009)
9. Caffarri S, Tibiletti T, Jennings R, Santabarbara S. 2014 A comparison between plant photosystem I and photosystem II architecture and functioning. *Curr. Protein Pept. Sci.* **15**, 296–331. (doi:10.2174/1389203715666140327102218)
10. Wraight CA, Clayton RK. 1974 The absolute quantum efficiency of bacteriochlorophyll photooxidation in reaction centres of *Rhodopseudomonas spheroides*. *BBA Bioenergy* **333**, 246–260. (doi:10.1016/0005-2728(74)90009-7)
11. Gobets B, Van Grondelle R. 2001 Energy transfer and trapping in photosystem I. *Biochim. Biophys. Acta Bioenergy* **1507**, 80–99. (doi:10.1016/S0005-2728(01)00203-1)
12. Croce R, Zucchelli G, Garlaschi FM, Bassi R, Jennings RC. 1996 Excited state equilibration in the photosystem I-light-harvesting I complex: P700 is almost isoenergetic with its antenna. *Biochemistry* **35**, 8572–8579. (doi:10.1021/bi960214m)
13. Nelson N. 2009 Plant photosystem I—the most efficient nano-photochemical machine. *J. Nanosci. Nanotechnol.* **9**, 1709–1713. (doi:10.1166/jnn.2009.SI01)
14. Nelson N, Ben-Shem A. 2005 The structure of photosystem I and evolution of photosynthesis. *Bioessays* **27**, 914–922. (doi:10.1002/bies.20278)
15. Cheng Y-C, Fleming GR. 2009 Dynamics of light harvesting in photosynthesis. *Annu. Rev. Phys. Chem.* **60**, 241–262. (doi:10.1146/annurev.physchem.040808.090259)
16. Lambert N, Chen YN, Cheng YC, Li CM, Chen GY, Nori F. 2013 Quantum biology. *Nat. Phys.* **9**, 10–18. (doi:10.1038/nphys2474)
17. Abramavicius D, Mukamel S. 2010 Quantum oscillatory exciton migration in photosynthetic reaction centers. *J. Chem. Phys.* **133**, 064510. (doi:10.1063/1.3458824)
18. Scholes GD, Fleming GR, Olaya-Castro A, Van Grondelle R. 2011 Lessons from nature about solar light harvesting. *Nat. Chem.* **3**, 764–774. (doi:10.1038/nchem.1145)
19. Frankcombe TJ. 2015 Explicit calculation of the excited electronic states of the photosystem II reaction centre. *Phys. Chem. Chem. Phys.* **17**, 3295–3302. (doi:10.1039/c4cp04468a)
20. Olson JM. 1981 Evolution of photosynthetic reaction centers. *Biosystems* **14**, 89–94. (doi:10.1016/0303-2647(81)90024-1)
21. Johansson M, Callaghan TV, Bosiö J, Åkerman HJ, Jackowicz-Korczynski M, Christensen TR. 2013 Rapid responses of permafrost and vegetation to experimentally increased snow cover in sub-arctic Sweden. *Environ. Res. Lett.* **8**, 035025. (doi:10.1088/1748-9326/8/3/035025)
22. Bellingeri M, Cassi D, Vincenzi S. 2014 Efficiency of attack strategies on complex model and real-world networks. *Phys. A Stat. Mech. Appl.* **340**, 79. (doi:10.1016/j.physa.2014.06.079)
23. Bellingeri M, Bodini A. 2013 Threshold extinction in food webs. *Theor. Ecol.* **6**, 143–152. (doi:10.1007/s12080-012-0166-0)
24. Bullmore E, Sporns O. 2009 Complex brain networks: graph theoretical analysis of structural and functional systems. *Nat. Rev. Neurosci.* **10**, 186–198. (doi:10.1038/nrn2575)
25. Zanin M, Lillo F. 2013 Modelling the air transport with complex networks: a short review. *Eur. Phys. J. Spec. Top.* **215**, 5–21. (doi:10.1140/epjst/e2013-01711-9)
26. Bellingeri M, Bevacqua D, Scotognella F, LU ZM, Cassi D. 2018 Efficacy of local attack strategies on the Beijing road complex weighted network. *Phys. A Stat. Mech. Appl.* **462**, 674–683. (doi:10.1016/j.physa.2018.06.127)
27. Agliari E, Barra A, Galluzzi A, Guerra F, Tantari D, Tavani F. 2015 Retrieval capabilities of hierarchical networks: from Dyson to Hopfield. *Phys. Rev. Lett.* **114**, 028103. (doi:10.1103/PhysRevLett.114.028103)
28. Onnela JP, Saramäki J, Hyvönen J, Szabó G, De Menezes MA, Kaski K, Barabási AL, Kertész J. 2007 Analysis of a large-scale weighted network of one-to-one human communication. *New J. Phys.* **9**, 179. (doi:10.1088/1367-2630/9/6/179)
29. Vicente-Serrano SM, Beguería S, Lorenzo-Lacruz J, Camarero JJ, López-Moreno JI, Azorin-Molina C, Revuelto J, Morán-Tejeda E, Sanchez-Lorenzo A. 2012 Performance of drought indices for ecological, agricultural, and hydrological applications. *Earth Interact.* **16**, 1–27. (doi:10.1175/2012EI000434.1)
30. Piccardi C, Tajoli L. 2018 Complexity, centralization, and fragility in economic networks. *PLoS ONE* **13**, e208265. (doi:10.1371/journal.pone.0208265)
31. Boccaletti S, Latora V, Moreno Y, Chavez M, Hwang DU. 2006 Complex networks: structure and dynamics. *Phys. Rep.* **424**, 175–308. (doi:10.1016/j.physrep.2005.10.009)
32. Bellingeri M, Bevacqua D, Scotognella F, Cassi D. 2019 The heterogeneity in link weights may decrease the robustness of real-world complex weighted networks. *Sci. Rep.* **9**, 10692. (doi:10.1038/s41598-019-47119-2)
33. Holme P, Kim BJ, Yoon CN, Han SK. 2002 Attack vulnerability of complex networks. *Phys. Rev. E Stat. Physics, Plasmas, Fluids, Relat. Interdiscip. Top.* **65**, 056109. (doi:10.1103/PhysRevE.65.056109)
34. Barrat A, Barthélemy M, Pastor-Satorras R, Vespignani A. 2004 The architecture of complex weighted networks. *Proc. Natl Acad. Sci. USA* **101**, 3747–3752. (doi:10.1073/pnas.0400087101)
35. Sporns O, Zwi JD. 2004 The small world of the cerebral cortex. *Neuroinformatics* **2**, 145–162. (doi:10.1385/NI:2:2:145)
36. Squartini T, Van Lelyveld I, Garlaschelli D. 2013 Early-warning signals of topological collapse in interbank networks. *Sci. Rep.* **3**, 3357. (doi:10.1038/srep03357)
37. Bellingeri M, Bodini A. 2016 Food web's backbones and energy delivery in ecosystems. *Oikos* **125**, 586–594. (doi:10.1111/oik.02244)
38. Bellingeri M, Bevacqua D, Scotognella F, Alfieri R, Cassi D. 2020 A comparative analysis of link removal strategies in real complex weighted networks. *Sci. Rep.* **10**, 3911. (doi:10.1038/s41598-020-60298-7)
39. Sener MK, Lu D, Ritz T, Park S, Fromme P, Schulten K. 2002 Robustness and optimality of light harvesting in cyanobacterial photosystem I. *J. Phys. Chem. B* **106**, 7948–7960. (doi:10.1021/jp020708v)
40. Llansola-Portoles MJ, Pascal AA, Robert B. 2017 Electronic and vibrational properties of carotenoids: from *in vitro* to *in vivo*. *J. R. Soc. Interface* **14**, 20170504. (doi:10.1098/rsif.2017.0504)
41. Croce R, Van Amerongen H. 2014 Natural strategies for photosynthetic light harvesting. *Nat. Chem. Biol.* **10**, 492–501. (doi:10.1038/nchembio.1555)
42. Van Amerongen H, Van Grondelle R. 2001 Understanding the energy transfer function of LHCII, the major light-harvesting complex of green plants. *J. Phys. Chem. B* **124**, 5780–5787. (doi:10.1021/jp0028406)
43. Förster T. 1948 Zwischenmolekulare Energiewanderung und Fluoreszenz. *Ann. Phys.* **437**, 55–75. (doi:10.1002/andp.19484370105)
44. Şener MK, Jolley C, Ben-Shem A, Fromme P, Nelson N, Croce R, Schulten K. 2005 Comparison of the light-harvesting networks of plant and

cyanobacterial photosystem I. *Biophys. J.* **89**, 1630–1642. (doi:10.1529/biophysj.105.066464)

45. Şener M, Strümpfer J, Hsin J, Chandler D, Scheuring S, Hunter CN, Schulten K. 2011 Förster energy transfer theory as reflected in the structures of photosynthetic light-harvesting systems. *Chemphyschem.* **12**, 518–531. (doi:10.1002/cphc.201000944)
46. Hussain SA. 2009 An introduction to fluorescence resonance energy transfer (FRET). https://arxiv.org/abs/arXiv:0908.1815 [physics.gen-ph].
47. van Grondelle R, Bergström H, Sundström V, Gillbro T. 1987 Energy transfer within the bacteriochlorophyll antenna of purple bacteria at 77 K, studied by picosecond absorption recovery. *BBA Bioenergy* **894**, 313–326. (doi:10.1016/0005-2728(87)90201-5)
48. Orzechowska A, Fiedor J, Kulakowski P. 2020 Light energy driven nanocommunications with FRET in photosynthetic systems. *arXiv*, 1–28. https://arxiv.org/abs/arXiv:2003.01628 [physics.bio-ph].
49. Cinque G, Croce R, Holzwarth A, Bassi R. 2000 Energy transfer among CP29 chlorophylls: calculated forster rates and experimental transient absorption at room temperature. *Biophys. J.* **79**, 1706–1717. (doi:10.1016/S0006-3495(00)76423-X)
50. Bellingeri M, Agliari E, Cassi D. 2015 Optimization strategies with resource scarcity: from immunization of networks to the traveling salesman problem. *Mod. Phys. Lett. B* **49**, 1550180. (doi:10.1142/S0217984915501808)
51. Kühlbrandt W, Wang DN, Fujiyoshi Y. 1994 Atomic model of plant light-harvesting complex by electron crystallography. *Nature* **367**, 614–621. (doi:10.1038/367614a0)
52. Morosinotto T, Breton J, Bassi R, Croce R. 2003 The nature of a chlorophyll ligand in Lhca proteins determines the far red fluorescence emission typical of photosystem I. *J. Biol. Chem.* **278**, 49 223–49 229. (doi:10.1074/jbc.M309203200)
53. Morosinotto T, Mozzo M, Bassi R, Croce R. 2005 Pigment–pigment interactions in Lhca4 antenna complex of higher plants photosystem I. *J. Biol. Chem.* **280**, 20 612–20 619. (doi:10.1074/jbc.M500705200)
54. Albert R, Barabási AL. 2002 Statistical mechanics of complex networks. *Rev. Mod. Phys.* **74**, 47. (doi:10.1103/RevModPhys.74.47)
55. Latora V, Marchiori M. 2001 Efficient behavior of small-world networks. *Phys. Rev. Lett.* **87**, 198701. (doi:10.1103/PhysRevLett.87.198701)
56. Bellingeri M, Cassi D. 2018 Robustness of weighted networks. *Phys. A Stat. Mech. Appl.* **489**, 47–55. (doi:10.1016/j.physa.2017.07.020)
57. Freeman LC. 1978 Centrality in social networks conceptual clarification. *Soc. Netw.* **1**, 1978–1979. (doi:10.1016/0378-8733(78)90021-7)
58. Newman M. 2010 *Networks: an introduction*. Oxford, UK: Oxford University Press. (doi:10.1093/acprof:oso/9780199206650.001.0001)
59. Iyer S, Killingback T, Sundaram B, Wang Z. 2013 Attack robustness and centrality of complex networks. *PLoS ONE* **8**, e59613. (doi:10.1371/journal.pone.0059613)
60. Kume A, Akitsu T, Nasahara KN. 2018 Why is chlorophyll b only used in light-harvesting systems? *J. Plant Res.* **131**, 961–972. (doi:10.1007/s10265-018-1052-7)
61. Jennings RC, Croce R, Dona D, Garlaschi FM, Holzwarth AR, Rivadossi A, Zucchelli G. 1998 Photosystem I red spectral forms: diffusion limited energy transfer, optical reorganisation energy and absorption cross section. In *Photosynthesis: mechanisms and effects* (ed. G Garab), pp. 271–276. Dordrecht, The Netherlands: Kluwer Academic Publishers.
62. Rivadossi A, Zucchelli G, Garlaschi FM, Jennings RC. 1999 The importance of PS I chlorophyll red forms in light-harvesting by leaves. *Photosynth. Res.* **40**, 287–294. (doi:10.1023/a:1006236829711)
63. Croce R, van Amerongen H. 2020 Light harvesting in oxygenic photosynthesis: structural biology meets spectroscopy. *Science* **369**, aay2058. (doi:10.1126/science.aay2058)
64. Blankenship RE, Chen M. 2013 Spectral expansion and antenna reduction can enhance photosynthesis for energy production. *Curr. Opin. Chem. Biol.* **17**, 457–461. (doi:10.1016/j.cbpa.2013.03.031)
65. González-Rodríguez AM, Morales D, Jiménez MS. 2002 Leaf age effects on chlorophyll, Rubisco, photosynthetic electron transport activities and thylakoid membrane protein in field grown grapevine leaves. *J. Plant Physiol.* **159**, 799–803. (doi:10.1078/0176-1617-0597)
66. Beisel KG, Jahnke S, Hofmann D, Köppchen S, Schurr U, Matsubara S. 2010 Continuous turnover of carotenes and chlorophyll a in mature leaves of *Arabidopsis* revealed by $^{14}CO_2$ pulse-chase labeling. *Plant Physiol.* **152**, 2188–2199. (doi:10.1104/pp.109.151647)
67. Giri S, Shrivastava D, Deshmukh K, Dubey P. 2013 Effect of air pollution on chlorophyll content of leaves. *Curr. Agric. Res. J.* **1**, 93–98. (doi:10.12944/carj.1.2.04)
68. Haag J. 2019 *Molecular and biochemical enhancement of chlorophyll in sports turf*. Cincinnati, OH: Xavier University.
69. Perrine Z, Negi S, Sayre RT. 2012 Optimization of photosynthetic light energy utilization by microalgae. *Algal Res.* **1**, 134–142. (doi:10.1016/j.algal.2012.07.002)
70. Melis A. 2009 Solar energy conversion efficiencies in photosynthesis: minimizing the chlorophyll antennae to maximize efficiency. *Plant Sci.* **177**, 272–280. (doi:10.1016/j.plantsci.2009.06.005)
71. Polle JEW, Kanakagiri S, Jin ES, Masuda T, Melis A. 2002 Truncated chlorophyll antenna size of the photosystems—a practical method to improve microalgal productivity and hydrogen production in mass culture. *Int. J. Hydrogen Energy* **27**, 1257–1264. (doi:10.1016/S0360-3199(02)00116-7)
72. Gust D, Moore TA, Moore AL. 2009 Solar fuels via artificial photosynthesis. *Acc. Chem. Res.* **42**, 1890–1898. (doi:10.1021/ar900209b)